Open Access Full Text Article

ORIGINAL RESEARCH

Bio Framework-Derived Facile MoO₃-NiO-PdO-Pd Nanomaterial for Detoxification of Organic Pollutants

Irum Shaheen[1]
Khuram Shahzad Ahmad [ORCID][1]
Daoud Ali[2]
Mohammed HA Almarzouq[2]
SA Hussain[2]
S Manohrdas[2]

[1]Department of Environmental Sciences, Fatima Jinnah Women University, Rawalpindi, Pakistan; [2]Department of Zoology, College of Science, King Saud University, Riyadh, Saudi Arabia

Introduction: The catalytic behavior of metal oxide nanomaterials for removal of organic pollutants under dark ambient conditions, without any additional stimulant, is of great interest among the scientific community.

Methods: In this account, a nanomaterial of ternary metal oxides (MoO₃-NiO-PdO-Pd) was synthesized via greener approach and was explored for degradation of methyl orange in water environment in dark ambient conditions in comparison with light conditions. The biochemical species of *Abies pindrow* were treated with aqueous solution of precursor's salt following sol gel synthesis strategy. We further attuned morphology and chemistry of MoO₃-NiO-PdO-Pd by incorporating bioactive compounds of *A. pindrow*.

Result and Discussion: The bio-fabricated MoO₃-NiO-PdO-Pd revealed outstanding catalytic behavior with 92% degradation of methyl orange within 15 min in the dark at ambient temperature and pressure. Whereas, in the presence of visible light irritation, the catalyst degraded 97% of methyl orange in 15 min. According to the reaction kinetics of degradation, the catalysts illustrated good stability in light (R^2=0.93) as well as in dark conditions (R^2=0.98). Furthermore, the outstanding reusability and recyclability of the synthesized nanomaterial was observed for four runs of the experiment under dark and light conditions.

Conclusion: Therefore, *A. pindrow*-synthesized MoO₃-NiO-PdO-Pd nanocatalyst demonstrated significant potential for detoxification of organic pollutants for water remediation.

Keywords: biochemical template, ternary metal oxides, nano-structures, organic pollutants, dye degradation

Introduction

Over recent times, various chemical industries and factories have been considered as key sources of water pollution.[1–3] From the various industrial water pollutants, the organic dyes are the most widespread class of pollutants and are frequently released by textile and paper industries.[3–6] Protection of water bodies from such organic contaminants is the greatest challenge of twenty-first century for environmentalists and researchers. Methyl orange (MO) is the most common dye of textile industries and has extraordinary potential to cause severe health problems. It is a well known carcinogen pollutant[5–7] thus its elimination from the water is extremely important.[7–11]

The different strategies and/or technologies are reported to treat/remove MO from water environments.[2,3,8–11] One such greatly investigated techniques is catalysis, ie catalytic degradation of organic dyes. It is an efficient, simple and sustainable alternative approach among scientists for the treatment of organic dyes.[1,2,9–13]

Correspondence: Khuram Shahzad Ahmad
Email chemist.phd33@yahoo.com

Transition metal oxides have proven to be economic and suitable photocatalysts to remove the organic dyes.[10–17] Moreover, metal oxide nanocomposites and mixed metal oxide nanomaterials significantly enhance the photocatalytic ability by altering the optical properties and by introducing the surface oxygen atoms that inhibit charge carrier recombination for longer periods of time.[2,4,18,19] The functional groups such as hydroxyl and carboxyl in the metal oxide-based materials show greater hydrophilicity as well as negative charge densities to assist the degradation of organic pollutants in the hydro environment.[20] In previous studies such organic groups were achieved by graphene oxides, multiwalled carbon nanotubes, etc.[20,21,22] However, in the current study such groups were incorporated into metal oxide nanoparticles by economic, and efficient synthesizing fuel, which was procured from *Abies pindrow* Royle foliage. The foliar fuel based synthesis of nanomaterials is widely investigated and reported.[20,23–27]

The leaves of *A. pindrow*, both as a crude drug and as amalgams are being used in its various localities, as a traditional medicine to cure different diseases, for example, antispasmodic, stomachic, tonic, etc.[27,28] Its reported biomedical implementations well surmised that the plant foliar is rich in abundant phytochemicals[28–30] which have been successfully demonstrated as fuel for the synthesis of nanomaterials.[20,23–27] Nevertheless, the published literature about phytosynthesis of nanomaterials has limitations of unexplored mechanism, unidentified phytocapping agents and being limited to mono and binary metal oxide synthesis. The present manipulation is endeavoring to overcome the drawbacks in biosynthesis by synthesizing facile MoO_3-NiO-PdO-Pd mixed metal oxide nanomaterial using foliar chemicals of *A. pindrow* and subsequently identifying the bioorganic molecules in synthesized material by GC-MS. In our recent study we have synthesized the Co_3O_4 based nanocatalyst using *A. pindrow* leaves extract and in this report we have also demonstrated the phytochemistry of *A. pindrow*, using different spectroscopic and chromatographic techniques. These identified phytochemicals have huge potential as synthesizing agents for nanomaterial preparation and fabrication.[31] Inspired by previous work, in the present investigation *A. pindrow* phytochemicals have been explored for the synthesis of MoO_3-NiO-PdO-Pd ternary metal oxide nanomaterial. The functional groups related to phytochemicals were introduced into the MoO_3-NiO-PdO-Pd nanomaterial, to remove MO not merely by visible light irritations, but also without light stimulant, under ambient conditions,

(without any additional stimulating agent). We believed that the investigated greener synthesis will add phytospecies in the synthesized MoO_3-NiO-PdO-Pd material which will expressively enhance the photocatalytic and catalytic efficiencies of nanomaterials by their oxygen-carbon related functional groups.

Materials and Methods

Molybdenum acetate 97% pure ($Mo_2(O_2CCH_3)_4$), nickel acetate tetrahydrate 99% pure ($Ni(CH_3CO_2)_2 \cdot 4\ H_2O$) and palladium acetate (($Pd(CH_3COO)_2$) with 92% purity were purchased from Merck Millipore (Billerica, MA, USA). Deionized water was used as a solvent in the current experimentation. The phytochemical extract of leaves of *A. pindrow* was utilized as fuel (containing reducing-cum-stabilizing agents) for synthesis of nanomaterial.

Synthesis of MoO_3-NiO-PdO-Pd Catalyst

The present biomimetic synthesis route was designed by modifying reported sol gel methods.[31–35] Aqueous solutions of 40 mM $Mo_2(O_2CCH_3)_4$ (3.4 g), 10 mM $Ni(CH_3CO_2)_2 \cdot 4\ H_2O$ (2 g) and 10 mM ($C_4H_6O_4Pd$) (1.8 g) were prepared individually in 200 mL of deionized water. For complete dissolution, each precursor salt was stirred continuously at 550 rpm and room temperature, and then reaction mixtures were mixed together. The foliar bioorganic compounds of *A. pindrow* were extracted as described earlier,[31] and the prepared extract was utilized for synthesis of MoO_3-NiO-PdO-Pd nanomaterial. An aliquot of 20 mL of *A. pindrow* extract was added slowly into prepared mixed solution of precursors on continuous stirring at 80°C for two hours and then retained at room temperature in the dark for 24 h to complete the phytofunctionalization process. Hereafter, the inorganic–organic mixture with obvious brownish black precipitates, was evaporated at 98°C. The evaporated dried powder was kept at 450°C for four hours in a muffle furnace to procure pure MoO_3-NiO-PdO-Pd mixed metal oxides. The mechanism of the phytosynthesis has been explained in scheme 1. The phytocompounds being reducing agents, reduced the metal salts into pure metal. During this process they incorporated into the metal, and this phytometal complex was then calcinated (in air) to get the respective oxides. The calcined nanomaterials of MoO_3-NiO-PdO-Pd were tested for degradation of MO under ambient conditions (room temperature and air pressure) as well as in the presence of visible light following the methodology adopted to our recent studies.[31] In brief, 100 g of MO was dissolved in 100 mL of deionized water in 1 mg/mL ratio. Two
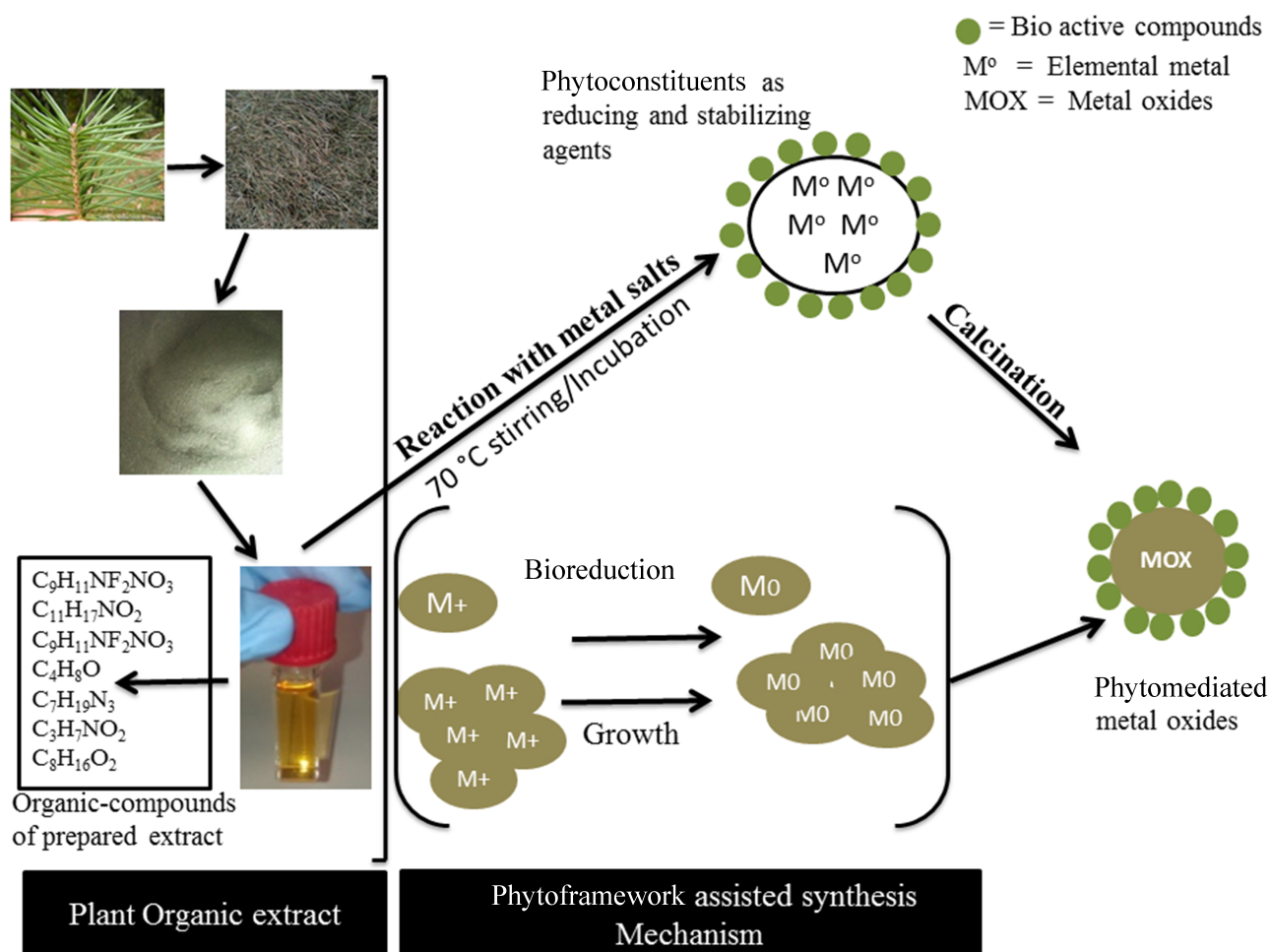
Scheme 1 Scheme of phytosynthesis of nanomaterials.

milligrams of the phytosynthesized nanomaterial was treated with 15 mL of prepared MO solution in dark and light conditions for 20 min. After completion of experiments, the catalyst was recovered and again subjected to the same experimental conditions to evaluate the reusability of photocatalyst. The degradation efficiency was calculated by the equation described previously.[31]

Characterization

The *A. pindrow* fabricated nanomaterial was analyzed by ultraviolet visible spectroscopy (UV-Vis.), gas chromatography coupled with the mass spectroscopy (GC-MS), Fourier transform infrared spectroscopy (FTIR), X-ray powder diffractometer (XRD), field emission scanning electron microscope (FE-SEM) and Raman spectroscopy. The details of instrumentation can be found in our previous studies.[25,31]

Results and Discussion
MoO_3-NiO-PdO-Pd Nanomaterial

The annealed phytofabricated MoO_3-NiO-PdO-Pd nanomaterial was analyzed by FTIR and the acquired spectra is shown in Figure 1A. The functional groups present in MoO_3-NiO-PdO-Pd were delineated at vibrational frequencies (cm^{-1}) of 2352.49, 1366.76 and 1115.9 indicating the presences of aromatics (C-C stretch) and aromatic amines (C-N) groups. The inset graph in Figure 1A shows M-O (M=Pd, Ni, Mo) bonds related to the metal oxides in fingerprint vibrational region (400–500 cm^{-1}).[36,37] Thus, the FTIR proposed the presence of carbon-related functional groups of phytofoliar compounds along with metal oxides.

The bioorganic species in MoO_3-NiO-PdO-Pd nanomaterial were monopolized by GC-MS of NIST library as revealed in Figure 1B. The existences of cyclobutanol (C_4H_8O) was identified in synthesized mixed metal oxides
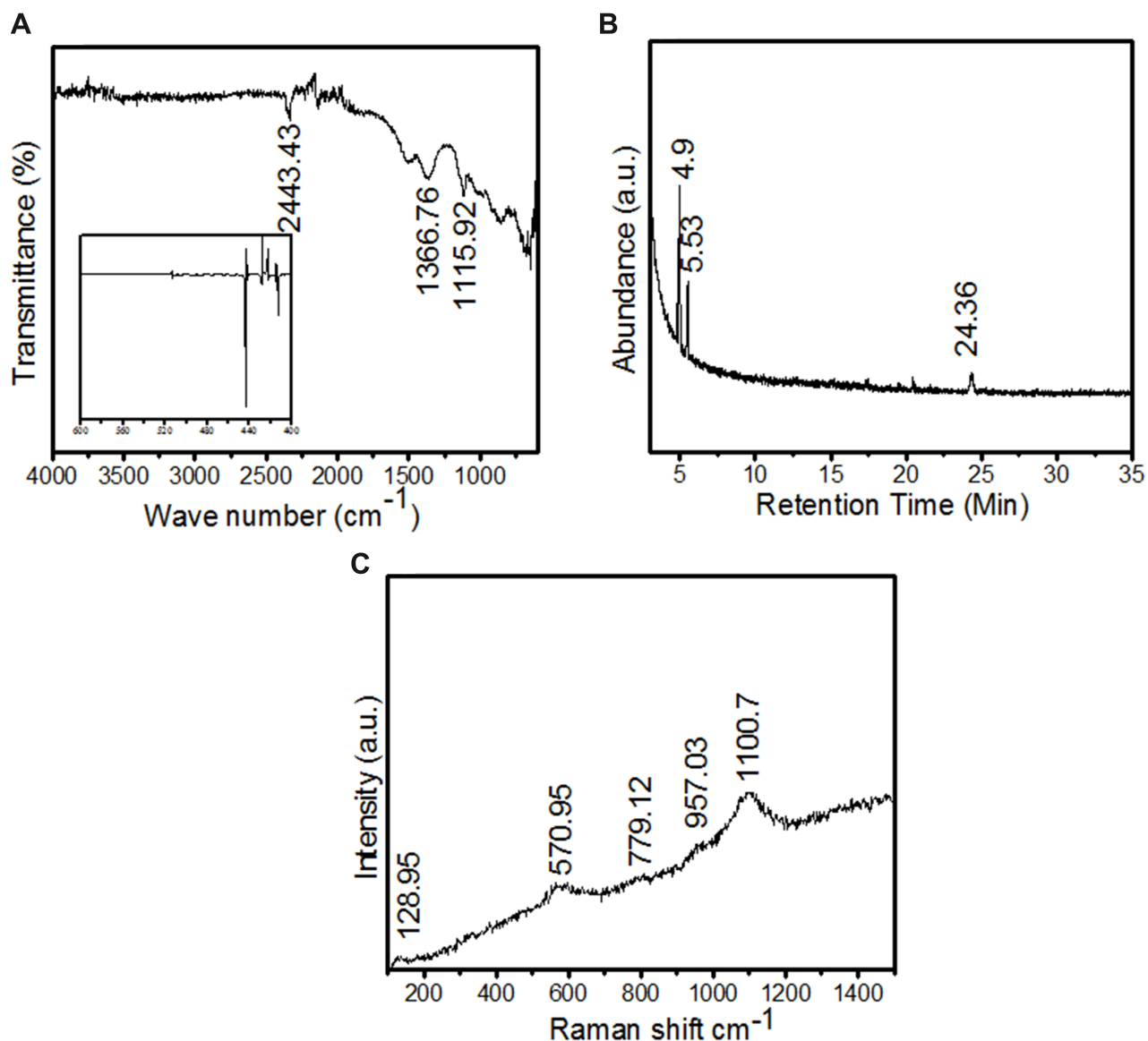
A

B

C

Figure 1 The demonstration of phytofunctional groups of MoO_3-NiO-PdO-Pd nanomaterial by (**A**) FTIR and (**B**) GC-MS and (**C**) Raman spectrum of MoO_3-NiO-PdO-Pd nanomaterial.

at retention times of 4.9, 5.4 and 24.3 as depicted in Figure 1B. The cyclobutanol was illustrated by the sharp prominent peaks of Figure 1B corresponding to the highest similarity index (SI) of the NIST library. Therefore, GCMS endorsed the carbonaceous compounds in synthesized material in well agreement with FTIR.

The compositional analysis of MoO_3-NiO-PdO-Pd nanomaterial was studied via Raman spectroscopy as presented in Figure 1C. In Figure 1C various vibrations can be observed at 300–3500 cm^{-1} corresponding to MoO_3, NiO, and PdO. The Raman scattering peaks greater than 1000 cm^{-1} in Figure 1C are proposing carbon-containing species of the plant foliar. These Raman observations are in good consistency to FTIR

results. However, MoO_3-NiO-PdO-Pd crystallinity and phase purity were revealed by XRD (Figure 2) and chemical compositional was studied by EDX (Figure 3).

Figure 2A shows the XRD analysis of foliar template-derived MoO_3-NiO-PdO-Pd nanomaterial. The diffraction peaks patterns of MoO_3 (*) in Figure 2A are according to ICSD 00–005-0508. The XRD revealed orthorhombic MoO_3 with the hkl planes as depicted as in Figure 2A having space group of Pbnm and the unit cell (a: 3.962, b: 13.858, c: 3.697 (Å)) parameters. The Figure 2A further revealed the presence of rhombohedral NiO (♦), tetragonal PdO (●) and cubic Pd (°) inconsistence with ICSD; 00–022-1189, 00–041-1107 and 00–005-0681 respectively. Moreover, the crystallite size of
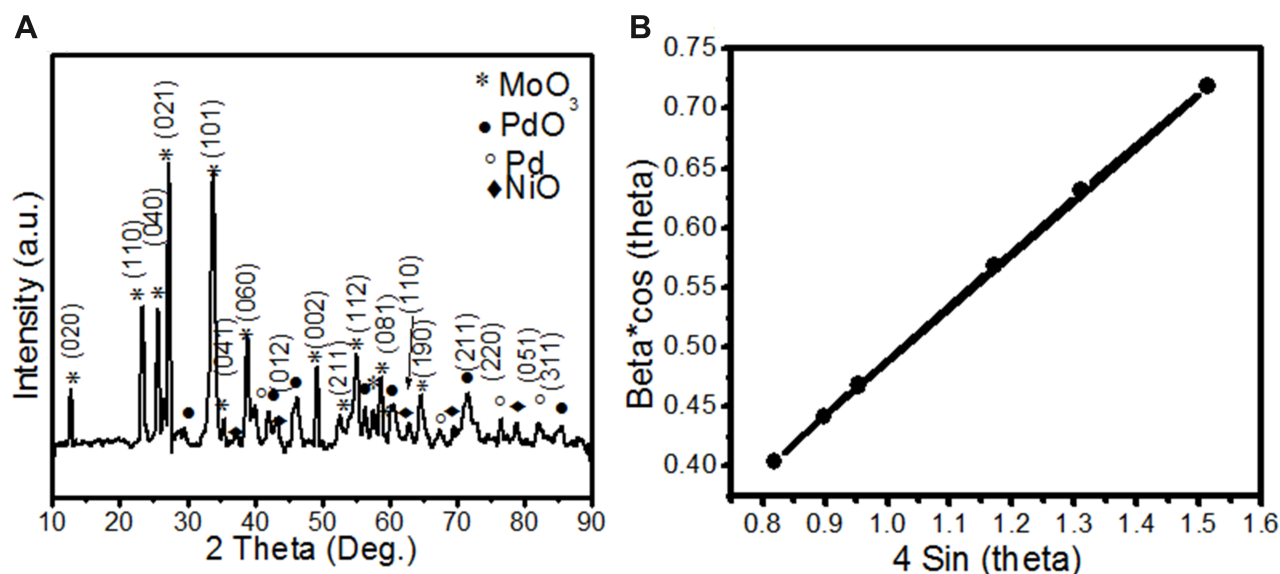
Figure 2 (**A**) The XRD diffraction patterns of foliar-synthesized MoO_3-NiO-PdO-Pd nanomaterial and (**B**) The plot of $4\sin\theta$ vs and $Beta*\cos\theta$ of synthesized nanomaterial using Williamson–Hall (W–H) equation.

MoO_3- NiO-PdO-Pd was calculated as 37.2 nm (±2.5 nm) according following Debye–Scherrer's equation;

$$D = (K\lambda)/(\beta\ cos\ \theta) \qquad (1)$$

Where, K is the shape factor, λ is wavelength of X-rays and β is full width at half maximum of peak intensity (in Rad).[38,39] In addition, the Williamson–Hall (W–H) equation was also used to calculate the crystalline size.[39,40]

$$\beta\ cos\ \theta = \frac{K\lambda}{D} + 4E*Sin\ \theta \qquad (2)$$

Where, E is stain (which is the slope), while D=K*λ/intercept. The W–H method was further used to draw size-strain plot (SSP) of synthesized nanomaterial as shown in Figure 2B. The SSP is a plot of $4\sin\theta$ vs and $\beta*\cos\theta$ and was draw using Gaussian model. By the linear fit to data, crystalline size (D) was determined from y-intercept, and the E, from slope of the fit and was found as 39.40 nm. Thus, according to XRD synthesized nanomaterial consists of three species NiO, Pd, and MoO_3. EDX spectrum (Figure 3C) strongly support the XRD results, describing the composition of fabricated material as Mo, Ni, Pd, O and C. According to atomic rations of Mo, Pd, and O, nanomaterial is classified as mixed metal oxides. The EDX shown the significant percentage of carbon indicating the stabilization of MoO_3-NiO-PdO-Pd by *A. pindrow* phytochemicals.

The FE-SEM of synthesized MoO_3-NiO-PdO-Pd were presented in Figure 3A and B. MoO_3-NiO-PdO-Pd nanomaterial was observed as nearly octahedral particles having uniform arrangement and regular structure. Accordingly, by FE-SEM uniformly arranged octahedral phytoframework-derived MoO_3-NiO-PdO-Pd nanomaterial were found. The minimum agglomeration of particle can also be seen in Figure 3A and B which is proposing the role of phyto-organic compounds as reducing-cum-stabilizing agents, which stabilized the nanoparticles to prevent them from agglomeration.

Catalytic Activity of MoO_3-NiO-PdO-Pd to Degrade MO

The catalytic potential of foliar fuel synthesized nanomaterial was investigated for degradation of the dye (MO) in the water assisted by visible light and also under the dark environmental condition. A blank solution was also tested in comparison with MoO_3-NiO-PdO-Pd nanocatalyst in order to evaluate the exact catalytic efficiency of synthesized material. The starting amount of MO in deionized water was 1 mg/mL and the nanomaterial loading was 2 mg/15 mL while the UV absorbance was recorded at different time intervals ranging between 0 and 20 minas presented in Figure 4. Consistent with the published literature,[2–10] in the present work, the degradation calibration graphs were prepared by taking the λ_{max} after 2, 5, 10, and 15 minas given in Figure 4.

In Figure 4A and B, a sharp and broad absorbance peak was found at 464 nm with minor vibration at 272 nm. It can be seen in Figure 4A that initially the absorbance band was deviated from 464 nm and recorded at 424 nm indicating the
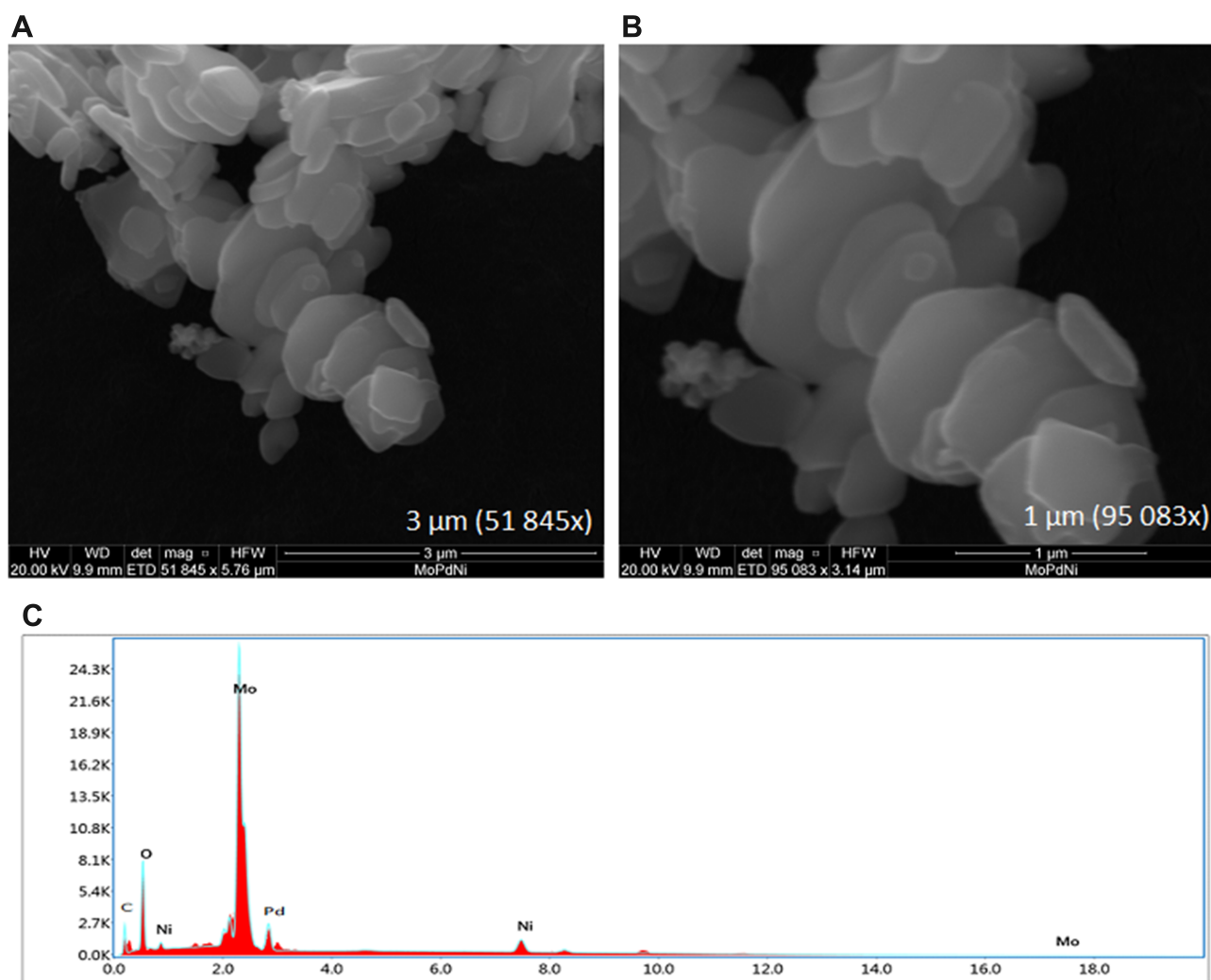
A

B

3 μm (51 845x)

HV	WD	det	mag □	HFW
20.00 kV	9.9 mm	ETD	51 845 x	5.76 μm

3 μm

MoPdNi

1 μm (95 083x)

HV	WD	det	mag □	HFW
20.00 kV	9.9 mm	ETD	95 083 x	3.14 μm

1 μm

MoPdNi

C

Figure 3 The morphology of foliar fueled MoO_3-NiO-PdO-Pd nanomaterial by FE-SEM at (**A**) 3 μm, (**B**) 1 μm and (**C**) Elemental analysis of MoO_3-NiO-PdO-Pd via energy-dispersive X-ray spectroscopy.

immediate reaction and activation of phytostabilized nanomaterial due to solar light irradiation along with MO. The synthesized material has incorporated foliar organic species which responded to the light irradiations. However, after that λ_{max} was recorded at 464 nm which was well maintained for the remaining readings. The exact peak was found in absorption spectra of MO (without catalyst) and has been delineated as Figure S2. It can be seen in the Figure S-1 that even after 15 min the color of the bank dye solution remained same. No change in the color of the MO solution was observed in the light (Figure C-S1) as well as in dark conditions (Figure D-S1) within 15 min without nanomaterial. Whereas, in the presence of synthesized catalyst complete decolorization of MO was observed simulated by solar irradiations (Figure B-S1). The Figure A S1 illustrated near to transparent color of the MO solution with MoO_3-NiO-PdO-

Pd nanomaterial without any stimulants, in the dark environmental conditions. This showed that decolorization was only due to catalytic activity of MoO_3-NiO-PdO-Pd, however, visible light irradiations were found to enhance degradation of MO by MoO_3-NiO-PdO-Pd. The absorption at 464 nm in Figure 4A and B is corresponding to azo bonds due to n--π*transition.[1] In the current study, as reaction time increased, the absorbance intensity at λ_{max} was observed to be considerably decreased, as depicted by Figure 4A and B which indicated the breakage of azo bond by foliar synthesized nanocatalyst under dark ambient conditions as well as under solar irradiation. The weak absorption band at 272 nm may be attributed to organic intermediates interferences of the azo bond and of bioorganic compounds of template. Based on the UV–Vis spectral observations (Figure 4A), it can be seen that the synthesized catalyst revealed efficient
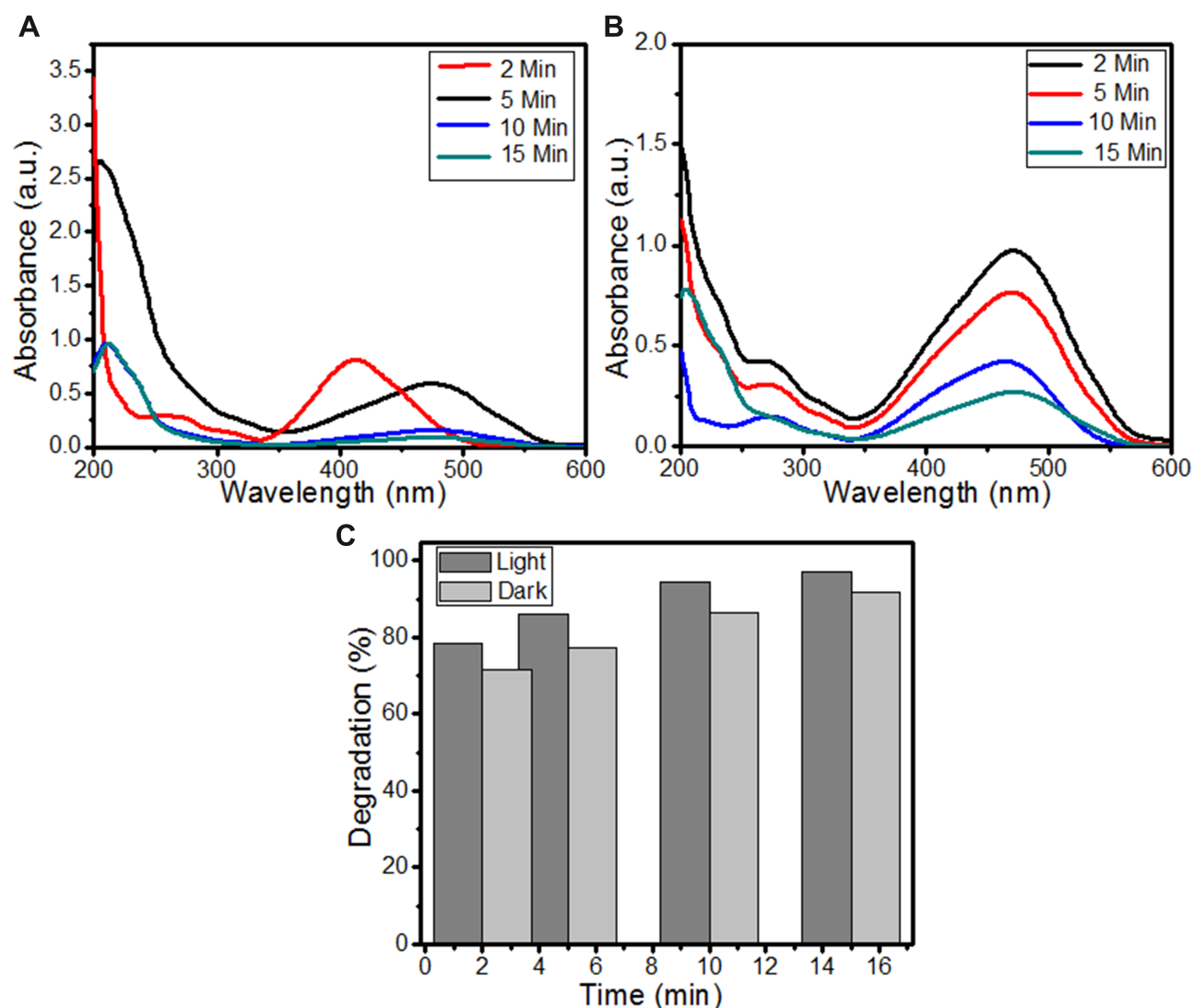
Figure 4 (**A**) UV Vis spectrum of MO/MoO$_3$-NiO-PdO-Pd solution in the presences of solar light, (**B**) absorption spectrum of MO/MoO$_3$-NiO-PdO-Pd in dark conditions, and (**C**) the degradation percentages of MO by MoO$_3$-NiO-PdO-Pd nanomaterial.

reduction of absorbance bands stimulated by light radiation compared to without light source (Figure 4B). While notable reduction in absorbance peaks was still achieved under dark conditions compared to blank sample where no reduction of azo bond was observed until 15 min (Figure S2). In Figure 4A, MoO$_3$-NiO-PdO-Pd nanocatalyst shows significant reduction in absorbance in the light as well as in dark conditions as shown in Figure 4B. The Figure 4A further presented the complete breakage of the azo bond after 15 min in light conditions. Not only did the peaks associated with azo bond disappear, but other peaks (below 300 nm) also disappeared in Figure 4B until 15 min, demonstrating the efficient behavior of MoO$_3$-NiO-PdO-Pd as photocatalyst. However, the absorbance of MoO$_3$-NiO-PdO-Pd (in both experimental

conditions of light and dark) is exceedingly less than absorption of blank solution which is given in Figure S2.

Using the UV data, against different time intervals, the degradation efficiency of foliar mediated catalyst was determined and delineated as shown in Figure 4C and in Table 1 while the self-degradation efficiency of MO, without nanomaterial, is given in Table 1 and in Figure S2. As can be seen from Table 1 and Figure 4C, MoO$_3$-NiO-PdO-Pd showed 94% efficiency to degrade MO in light while 86% efficiency of the nanomaterial was retained without light stimulants up to 10 min. After 15 min degradation was enhanced to 97% and 92% in the visible light and in the dark condition respectively. This outstanding catalytic behavior of MoO$_3$-NiO-PdO-Pd was attributed to

nanostructures as shown in Figure 3A and B. Table 1 also revealed that at five minutes, 77% degradation efficiency was observed even without light irradiation and 86% efficiency of nanomaterial was revealed by light stimulation at five minutes. These results show that although synthesized catalyst demonstrated excellent behavior in dark conditions, still the catalytic efficiency was greatly enhanced due to solar light. Therefore, outstanding potential of MoO_3-NiO-PdO-Pd was revealed even in dark condition. The nanostructures and incorporated carbon-containing groups were efficiently increase catalytic performance of MoO_3-NiO-PdO-Pd catalyst, even without any light or chemical stimulants compared to reported studies.[38,39,41–44] Xue et al reported the 95% degradation of MO under visible light radiation by TiO based nanocatalyst in five hours.[45] In an another study, Zhang et al synthesized the $Cu_{2-x}S$ based diatom nanocatalyst and demonstrated its 96.9% degradation efficiency for MO in 40 min under UV Visible light.[46] Thus, the organic compound-derived MoO_3-NiO-PdO-Pd is an excellent catalyst for both light and dark conditions toward MO degradation in minimum time.

From Figure 4, organic framework-derived MoO_3-NiO-PdO-Pd catalyst revealed efficient catalytic behavior within 15 min as photocatalyst and without photo degradation. It can be seen that within 10 min no major influence of light was observed on the catalytic activity of biotemplate MoO_3-NiO-PdO-Pd nanomaterial. Such behavior of catalyst (in dark conditions) is suggesting the catalytic wet oxidation process (CWO).[41] However, complete removal of MO within 15 min by light as the stimulant was due to carboncontaining phytomaterials which are reported as efficient electron acceptors for the metal oxides which are strong electron donors.[41–44] Consequently, carbonaceous bioactive compounds, as exposed by GCMS, efficiently assisted the transport of solar

light-generated electrons/holes in opposed direction to persist electrons lifetime to employ the light more efficiently.

Figure 5 illustrates the plot of ln (C_t/C_o) vs time to determine the reaction kinetics. As shown in Figure 5, the degradation of MO was found to have first order kinetics. The regression value for photocatalytic degradation was 0.92 whereas the catalyst revealed regression value of 0.98 in dark catalytic conditions. Hence, the regression analysis, MoO_3-NiO-PdO-Pd illustrated the preliminary stability of the phytosynthesized catalyst.

The reusability of the synthesized nanocatalyst was tested for four runs of experiments by recovering the material through centrifuging at 6000 rpm for 10 min followed by washing and 80°C drying. The reusability experimentation revealed no significant change in absorbance intensities until the fourth run as presented in Figure 6, subsequently no notable change in efficiency of the catalyst was observed for degradation of MO. MoO_3-NiO-PdO-Pd nanocomposite in the dark as well as in light was observed to be stable until four runs (Figure 6) with significant degradation efficiencies of 96.5% and 90.1% until the fourth experimental cycle in the presence of solar light and in dark conditions respectively. Srikhaow and Smith investigated the reusability of $Cu_2(OH)_3NO_3/ZnO$ and by the same recovery process they demonstrated constant efficiency of catalyst till three runs.[41] Kadam et al reported 91% degradation efficiency of ZnO/Ag_2O nanocomposites after three runs.[42] Ta et al, recovered AgNWs/ZnO NRs/AgNPs catalyst by centrifugation and washing for four experiments with 98% degradation of MO within 40 min.[2]

Nevertheless, in the current research a higher degradation efficiency of MoO_3-NiO-PdO-Pd nanocomposite was achieved in 15 min for four runs. The excellent stability was attributed to the presences of additional oxygen and carbon compounds of phytotemplate as endorsed by Figure 1. However, in the present study after repeating fourth experimental run, the catalyst efficiency was more in the presence of solar irradiation compared to ambient (dark) conditions as expressed in Figure 6A and B, demonstrating that MoO_3-NiO-PdO-Pd nanocomposite was intact and behaved as a photostable catalyst. The stability and reusability of catalytic material is tremendously important for its large-scale practical application.[41–43]

Possible Mechanisms for Catalytic Degradation of MO

In the present study, two contrasting experimental conditions were investigated for catalytic degradation of MO
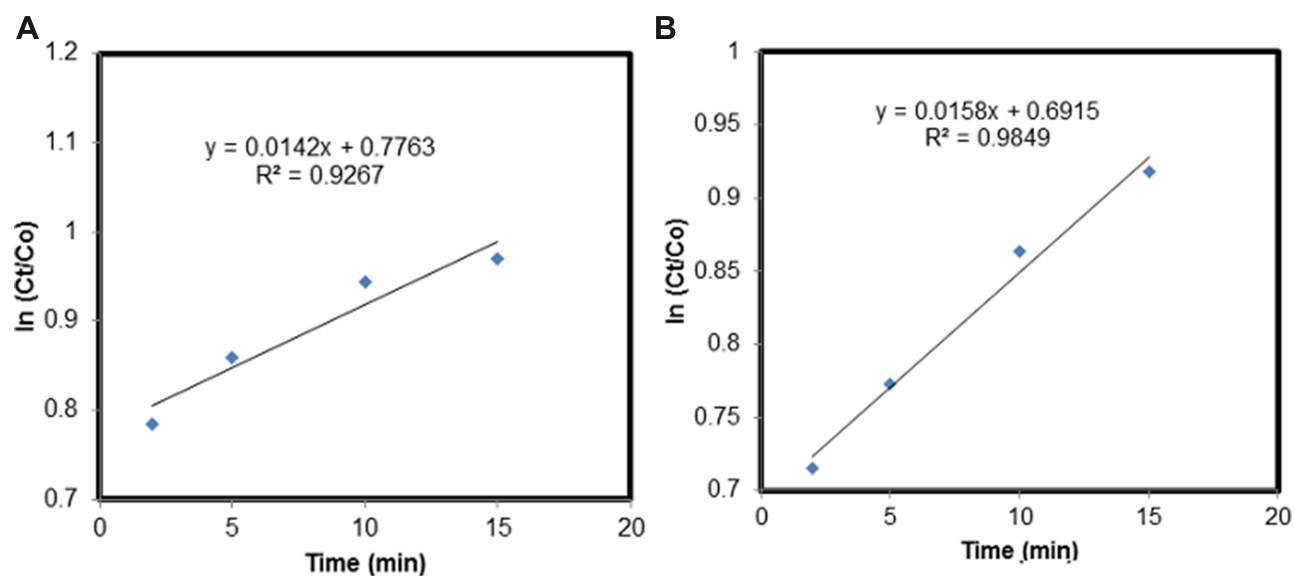
Table I The Degradation Efficiency of Synthesized Nanomaterial in Comparison with Blank

Time (Minutes)	Degradation Efficiency (%)		Self-degradation of MO (Bank Sample) (%)	
	Assisted by Light	Ambient Dark Catalysis	Assisted by Light	Ambient Dark Catalysis
2	78.5	71.53	0	0
5	85.9	77.4	2	0
10	94.5	86.4	5	2
15	97.4	91.8	5	0.5

A

B

Figure 5 A plot of ln (C_t/C_o) vs time presenting the reaction kinetic of MoO_3-NiO-PdO-Pd (**A**) in presence of light, and (**B**) in ambient dark conditions.

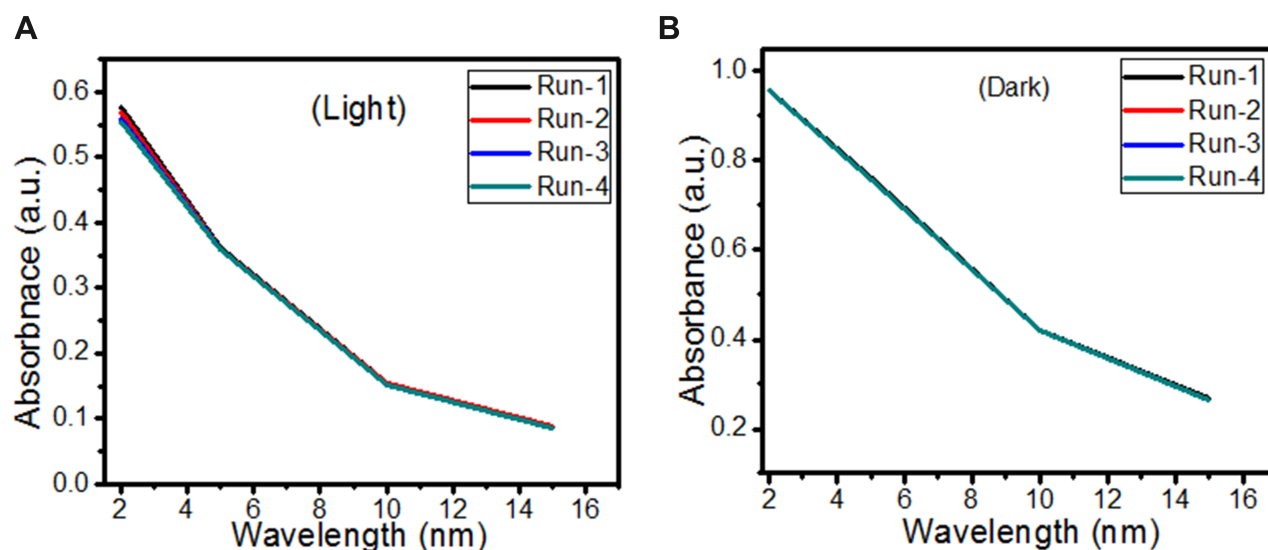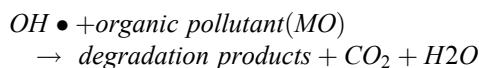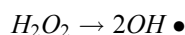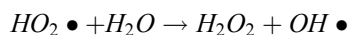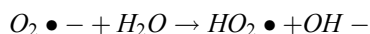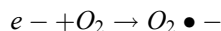**A**

B

Figure 6 Stability of catalyst for MoO_3-NiO-PdO-Pd nanocomposite (**A**) under light conditions, and (**B**) under dark conditions.

pollutant from an aqueous environment. The synthesized catalyst was investigated to degrade MO in the presence of visible solar light irradiation and in dark ambient conditions. The control (bank) sample of dye was also subjected to same experimental conditions to verify the catalytic efficiency of the investigated material. As revealed by control experiments, no change in the absorbance was observed indicating the degradation was attributed merely to the synthesized nanocatalyst.

It can be seen from Figure 4A and B that in two minutes no major difference in the degradation efficiency

of nanomaterial was observed in light and dark conditions. The nanomaterial revealed quite higher (~92%) degradation percentage of MO in 15 min in the dark experimental conditions suggesting the mechanism of CWO to degrade MO in ambient dark conditions. According to the CWO process, MO undergo aerial oxidation process over the nanomaterial.[41,43] The CWO depends on the increased oxygen vacancies to degrade organic pollutant in the water. The combination of ternary metal oxides (MoO_3, PdO, NiO) has increased the oxygen concentration which then binds the electrons (generated from the nanocatalyst)
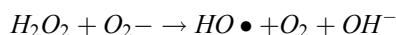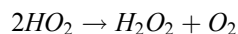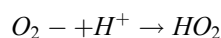
to produce superoxide radical anion $\bullet O_2^-$. The electrons of the conduction bands of metal oxide nanomaterial reacted with the O_2 and H_2O at the catalyst surface generating $\bullet OH$ and H_2O_2. Thus, increased number of oxygen species reacted with the electrons of the metal oxides and degraded MO.[41,43]

$$e - + O_2 \rightarrow O_2 \bullet -$$

$$O_2 \bullet - + H_2O \rightarrow HO_2 \bullet + OH -$$

$$HO_2 \bullet + H_2O \rightarrow H_2O_2 + OH \bullet$$

$$H_2O_2 \rightarrow 2OH \bullet$$

$$h + + OH \rightarrow OH \bullet$$

$$OH \bullet + organic\ pollutant(MO)$$
$$\rightarrow \ degradation\ products + CO_2 + H2O$$

However, maximum (97%) degradation of MO in presences of solar light irradiations was due to the fact that carbon species are competent electron acceptors while semiconductor metal oxides are efficient electron donors.[44] The GC-MS (Figure 1B) and FTIR (Figure 1A) vividly demonstrated the presence of carbon-based phytochemicals which facilitated the transport of light irritation-generated charge carriers (in opposite directions) to extend the electrons lifetime. These electrons then employed visible light irradiation with the greater efficiency. The photodegradation was due to coupling of semiconductor metal oxides and carbon materials which inhabited the e– and h$^+$ recombination and efficiently facilitated the charge separation in the presences of solar light irradiations, so the enhanced photocatalytic activity of nanomaterial was observed for the degradation of MO. As per proposed mechanism, initially the MoO$_3$-NiO-PdO-Pd nanomaterial was activated by visible light irradiation;

$$Physyntheized\ nanomaterial + hv \rightarrow e - + h +$$

$$e - + O_2 \rightarrow O_2 -$$
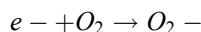
Then, oxidation-reduction reactions were carried out to degrade MO;

$$O_2 - + H^+ \rightarrow HO_2$$

$$2HO_2 \rightarrow H_2O_2 + O_2$$

$$H_2O_2 + O_2 - \rightarrow HO \bullet + O_2 + OH^-$$

$$HO \bullet + organic dye \rightarrow CO_2 + H_2O$$

Consequently, ternary metal oxides and incorporated carbon based phytoconstituents efficiently increased the catalytic performance of MoO$_3$-NiO-PdO-Pd catalyst, even without any light or chemical stimulants with high reusability.

Conclusion

In summary, a distinctive strategy of phytosynthesis was reported to fabricate mixed metal oxide-based nanocatalyst. We have not only synthesized nanostructures of MoO$_3$-NiO-PdO-Pd but have efficiently functionalized the chemistry of MoO$_3$-NiO-PdO-Pd via organic compounds. The bioorganic compounds enhanced efficiency of the fabricated catalyst to degrade MO in the minimum time. The MoO$_3$-NiO-PdO-Pd achieved the efficiency of 97% and 92% under light and dark conditions respectively to remove MO in the aqueous environment. This degradation efficiency was achieved within 15 min. Furthermore, a moderate degradation percentage of 86 and 77% were still retained at lower time interval of five minutes in the light and dark conditions respectively. Such catalytic excellent behavior was endorsed to the superior effects of nanostructures, and increased reactive species due to mixed metal oxides and to carbon-containing phytofunctional groups in ternary metal oxides. Thus, our study has provided an easy, eco-friendly, and low cost synthesis route to developed heterogeneous nanocatalyst to degrade organic pollutants in waterbodies on an industrial scale.

Acknowledgments

Disclosure

The authors report no conflicts of interest in this work.

References

1. Zhong W, Jiang T, Dang Y, et al. Mechanism studies on methyl orange dye degradation by perovskite-type LaNiO3-δ under dark ambient conditions. *Appl Catal A Gen*. 2018;549:302–309. doi:10.1016/j.apcata.2017.10.013

2. Ta QTH, Cho E, Sreedhar A, Noh J-S. Mixed-dimensional, three-level hierarchical nanostructures of silver and zinc oxide for fast photocatalytic degradation of multiple dyes. *J Catal*. 2019;371:1–9. doi:10.1016/j.jcat.2019.01.023

3. Suryavanshi RD, Mohite SV, Bagade AA, Shaikh SK, Thorat JB, Rajpure KY. Nanocrystalline immobilised ZnO photocatalyst for degradation of benzoic acid and methyl blue dye. *Mater Res Bull*. 2018;101:324–333. doi:10.1016/j.materresbull.2018.01.042

4. Adeleke JT, Theivasanthi T, Thiruppathi M, Swaminathan M, Akomolafe T, Alabi AB. Photocatalytic degradation of methylene blue by ZnO/NiFe2O4 nanoparticles. *Appl Surf Sci*. 2018;455:195–200. doi:10.1016/j.apsusc.2018.05.184

5. Znad H, Abbas K, Hena S, Awual MR. Synthesis a novel multi-lamellar mesoporous TiO2/ZSM-5 for photo-catalytic degradation of methyl orange dye in aqueous media. *J Environ Chem Eng*. 2018;6 (1):218–227. doi:10.1016/j.jece.2017.11.077

6. He K, Chen G, Zeng G, et al. Three-dimensional graphene supported catalysts for organic dyes degradation. *Appl Catal A Environ*. 2018;228:19–28.

7. Weeramonkhonlert V, Srikhaow A, Smith SM. Formation of copper hydroxy double salts derived from metal oxides and their catalytic activity in degradation of methyl orange. *Ceram Int*. 2019;45 (1):993–1000. doi:10.1016/j.ceramint.2018.09.278

8. Shen Z, Zhou H, Chen H, Xu H, Feng C, Zhou X. Synthesis of nano-zinc oxide loaded on mesoporous silica by coordination effect and its photocatalytic degradation property of methyl orange. *Nanomaterials*. 2018;8(5):317. doi:10.3390/nano8050317

9. Nguyen VN, Tran DT, Nguyen MT, et al. Enhanced photocatalytic degradation of methyl orange using ZnO/graphene oxide nanocomposites. *Res Chem Intermed*. 2018;44(5):3081–3095. doi:10.1007/s11164-018-3294-3

10. Mohammed SA, Al Amouri L, Yousif E, et al. Synthesis of NiO: V2O5 nanocomposite and its photocatalytic efficiency for methyl orange degradation. *Heliyon*. 2018;4(3):e00581. doi:10.1016/j.heliyon.2018.e00581

11. Nasirian M, Mehrvar M. Photocatalytic degradation of aqueous methyl orange using nitrogen-doped TiO2 photocatalyst prepared by novel method of ultraviolet-assisted thermal synthesis. *J Environ Sci*. 2018;66:81–93. doi:10.1016/j.jes.2017.05.032

12. Rani M, Shanker U. Sun-light driven rapid photocatalytic degradation of methylene blue by poly (methyl methacrylate)/metal oxide nanocomposites. *Colloids Surf A*. 2018;559:136–147. doi:10.1016/j.colsurfa.2018.09.040

13. Lin Y, Wan H, Chen F, Liu X, Ma R, Sasaki T. Two-dimensional porous cuprous oxide nanoplatelets derived from metal–organic frameworks (MOFs) for efficient photocatalytic dye degradation under visible light. *Dalton Trans*. 2018;47(23):7694–7700. doi:10.1039/C8DT01117F

14. Vidyasagar D, Ghugal SG, Kulkarni A, et al. Silver/Silver (II) oxide (Ag/AgO) loaded graphitic carbon nitride microspheres: an effective visible light active photocatalyst for degradation of acidic dyes and bacterial inactivation. *Appl Catal B*. 2018;221:339–348. doi:10.1016/j.apcatb.2017.09.030

15. Pan D, Ge S, Zhao J, et al. Synthesis, characterization and photocatalytic activity of mixed-metal oxides derived from NiCoFe ternary layered double hydroxides. *Dalton Trans*. 2018;47(29):9765–9778. doi:10.1039/C8DT01045E

16. Hunge YM, Yadav AA, Mathe VL. Ultrasound assisted synthesis of WO3-ZnO nanocomposites for brilliant blue dye degradation. *Ultrason Sonochem*. 2018;45:116–122. doi:10.1016/j.ultsonch.2018.02.052

17. Pascariu P, Cojocaru C, Olaru N, Airinei A. Photocatalytic activity of ZnO–SnO2 ceramic nanofibers for RhB dye degradation: experimental design, modeling, and process optimization. *Phys Status Solidi B*. 2019;256(5):1800474. doi:10.1002/pssb.201800474

18. Alam U, Khan A, Ali D, Bahnemann D, Muneer M. Comparative photocatalytic activity of sol–gel derived rare earth metal (La, Nd, Sm and Dy)-doped ZnO photocatalysts for degradation of dyes. *RSC Adv*. 2018;8(31):17582–17594. doi:10.1039/C8RA01638K

19. Kale G, Arbuj S, Kawade U, Rane S, Ambekar J, Kale B. Synthesis of porous nitrogen doped zinc oxide nanostructures using a novel paper mediated template method and their photocatalytic study for dye degradation under natural sunlight. *Mater Chem Front*. 2018;2 (1):163–170. doi:10.1039/C7QM00490G

20. Banerjee S, Benjwal P, Singh A, et al. Zinc oxide nanoparticles: a review of their biological synthesis, antimicrobial activity, uptake, translocation and biotransformation in plants. *J Mater Sci*. 2018;53 (1):185–201. doi:10.1007/s10853-017-1544-1

21. Labhane PK, Sonawane SH, Sonawane GH, Patil SP, Huse VR. Influence of Mg doping on ZnO nanoparticles decorated on graphene oxide (GO) crumpled paper like sheet and its high photo catalytic performance under sunlight. *J Phys Chem Solid*. 2018;114:71–82. doi:10.1016/j.jpcs.2017.11.017

22. Zhang X, He X, Kang Z, Cui M, Yang D-P, Luque R. Waste eggshell-derived dual-functional CuO/ZnO/Eggshell nanocomposites: (photo)catalytic reduction and bacterial inactivation. *ACS Sustain Chem Eng*. 2019;7(18):15762–15771. doi:10.1021/acssuschemeng.9b04083

23. Rolim WR, Pelegrino MT, de Araújo Lima B, et al. Green tea extract mediated biogenic synthesis of silver nanoparticles: characterization, cytotoxicity evaluation and antibacterial activity. *Appl Surf Sci*. 2019;463:66–74. doi:10.1016/j.apsusc.2018.08.203

24. Hussain A, Oves M, Alajmi MF, et al. Biogenesis of ZnO nanoparticles using pandanus odorifer leaf extract: anticancer and antimicrobial activities. *RSC Adv*. 2019;9(27):15357–15369. doi:10.1039/C9RA01659G

25. Shaheen I, Ahmad KS, Zequine C, Gupta RK, Thomas A, Malik MA. Organic template-assisted green synthesis of CoMoO 4 nanomaterials for the investigation of energy storage properties. *RSC Adv*. 2020;10 (14):8115–8129. doi:10.1039/C9RA09477F

26. Kumar HK, Mohana NC, Nuthan BR, et al. Phyto-mediated synthesis of zinc oxide nanoparticles using aqueous plant extract of Ocimum americanum and evaluation of its bioactivity. *SN Appl Sci*. 2019;1 (6):651. doi:10.1007/s42452-019-0671-5

27. Singh J, Dutta T, Kim KH, Rawat M, Samddar P, Kumar P. 'Green'synthesis of metals and their oxide nanoparticles: applications for environmental remediation. *J Nanobiotechnol*. 2018;16(1):84. doi:10.1186/s12951-018-0408-4

28. Kumar D, Kumar SA complete monographic study on abies pindrow royle aerial parts. *Indian J Pharm Sci*. 2018;79(6):1001–1007.

29. Majeed H, Bokhari TZ, Sherwani SK, Younis U, Shah MHR, Khaliq B. An overview of biological, phytochemical, and pharmacological values of abies pindrow. *J Pharmacogn Phytochem*. 2013;2:3.

30. Mushtaq S, Chaudhry MA, Rahman HMA. Calcium channels blocked activity: providing the basis for medicinal use of *Abies pindrow* in diarrhea and bronchitis. *Bangladesh J Pharmacol*. 2015;10(2):430–435. doi:10.3329/bjp.v10i2.22246

31. Shaheen I, Ahmad KS. Green synthesis of doped Co3O4 nano-catalysts using organic template for fast azo dyes degradation from aqueous environment. *J Chem Technol Biotechnol*. 2020.

32. Shao J, Zhou H, Zhu M, Feng J, Yuan A. Facile synthesis of metal-organic framework-derived Co3O4 with different morphologies coated graphene foam as integrated anodes for lithium-ion batteries. *J Alloys Compd*. 2018;768:1049–1057. doi:10.1016/j.jallcom.2018.07.290

33. Rezaee S, Shahrokhian S. Facile synthesis of petal-like NiCo/NiO-CoO/nanoporous carbon composite based on mixed-metallic MOFs and their application for electrocatalytic oxidation of methanol. *Appl Catal B Environ*. 2019;244:802–813.

34. Dolla TH, Pruessner K, Billing DG, et al. Sol-gel synthesis of Mn Ni1Co2O4 spinel phase materials: structural, electronic, and magnetic properties. *J Alloys Compd*. 2018;742:78–89. doi:10.1016/j.jallcom.2018.01.139

35. Moghaddam SV, Rezaei M, Meshkani F, Daroughegi R. Carbon dioxide methanation over Ni-M/Al2O3 (M: fe, CO, Zr, La and Cu) catalysts synthesized using the one-pot sol-gel synthesis method. *Int J Hydrogen Energy.* 2018;43(34):16522–16533. doi:10.1016/j.ijhydene.2018.07.013

36. Vinodha G, Cindrella L, Sithara V, Philip J, Shima PD. Synthesis, characterization, thermal conductivity and rheological studies in magnetite-decorated graphene oxide nanofluids. *J Nanofluids.* 2018;7(1):11–20. doi:10.1166/jon.2018.1435

37. Nauman A, Naz H, Li J, Zhu X, Liu P, Xiang B. Band gap engineering of transition metal (Ni/Co) codoped in zinc oxide (ZnO) nanoparticles. *J Alloys Compd.* 2018;744:90–95.

38. Shaheen I, Ahmad KS. Chromatographic identification of "green capping agents" extracted from Nasturtium officinale (Brassicaceae) leaves for the synthesis of MoO3 nanoparticles. *J Sep Sci.* 2020;43(3):598–605.

39. Mote VD, Purushotham Y, Dole BN. Williamson-hall analysis in estimation of lattice strain in nanometer-sized ZnO particles. *J Theor Appl Phys.* 2012;6(1):6. doi:10.1186/2251-7235-6-6

40. Zak AK, Majid WH, Abrishami ME, Yousefi R. X-ray analysis of ZnO nanoparticles by williamson–hall and size–strain plot methods. *Solid State Sci.* 2011;13(1):251–256. doi:10.1016/j.solidstatesciences.2010.11.024

41. Srikhaow A, Smith SM. Preparation of Cu2(OH)3NO3/ZnO, a novel catalyst for methyl orange oxidation under ambient conditions. *Appl Catal B.* 2013;130–131:84–92. doi:10.1016/j.apcatb.2012.10.018

42. Kadam A, Dhabbe R, Gophane A, Sathe T, Garadkar K. Template free synthesis of ZnO/Ag2O nanocomposites as a highly efficient visible active photocatalyst for detoxification of methyl orange. *J Photochem Photobiol B.* 2016;154:24–33. doi:10.1016/j.jphotobiol.2015.11.007

43. Wei S, Hu X, Liu H, Wang Q, He C. Rapid degradation of congo red by molecularly imprinted polypyrrole-coated magnetic TiO2 nanoparticles in dark at ambient conditions. *J Hazard Mater.* 2015;294:168–176. doi:10.1016/j.jhazmat.2015.03.067

44. Reddy KR, Gomes VG, Hassan M. Carbon functionalized TiO 2 nanofibers for high efficiency photocatalysis. *Mater Res Express.* 2014;1(1):015012. doi:10.1088/2053-1591/1/1/015012

45. Xue H, Chen Y, Liu X, et al. Visible light-assisted efficient degradation of dye pollutants with biomass-supported TiO2 hybrids. *Mater Sci Eng C.* 2018;82:197–203. doi:10.1016/j.msec.2017.08.060

46. Zhang X, Zhou J, Yang D-P, Chen S, Huang J, Li Z. Cu2-xS loaded diatom nanocomposites as novel photocatalysts for efficient photocatalytic degradation of organic pollutants. *Catal Today.* 2019;335:228–235. doi:10.1016/j.cattod.2018.11.047